minerals

MDPI

Article

Chlorine-Deficient Analog of Taseqite from Odikhincha Massif (Russia): Genesis and Relation with Other Sr-Rich Eudialyte-Group Minerals

Victor A. Zaitsev [1], Nikita V. Chukanov [2] and Sergey M. Aksenov [3,4,*]

[1] Vernadsky Institute of Geochemistry and Analytical Chemistry, Russian Academy of Sciences, 19 Kosygin Street, 119991 Moscow, Russia
[2] Institute of Problems of Chemical Physics, Russian Academy of Sciences, 142432 Chernogolovka, Russia
[3] Laboratory of Arctic Mineralogy and Materials Sciences, Russian Academy of Sciences, 14 Fersman Street, 184209 Apatity, Russia
[4] Geological Institute, Kola Science Centre, Russian Academy of Sciences, 14 Fersman Street, 184209 Apatity, Russia
* Correspondence: aks.crys@gmail.com

Abstract: Eudialyte-group minerals are important accessory minerals of peralkaline rocks of nepheline-syenite massifs and alkaline–ultramafic complexes. Here, we report the complex study of a eudialyte-group mineral (EGM) from peralkaline pegmatite of the alkaline-ultrabasic Odikhincha massif (Polar Siberia). The chemical composition of the studied EGM is intermediate between those of taseqite and eudialyte, with small admixtures of other members of the eudialyte group. The crystals of EGMs were formed during the postmagmatic stage in the temperature range of 300–350 °C and partly replaced by late eudialite along cracks during the zeolite stage (~230 °C). The chemical compositions, structural features and mineral association of the studied EGM are similar to those of Sr-Nb-dominant EGM found in other nepheline-syenite massifs, such as Khibiny, Lovozero and Pilansberg. The EGM studied in this work is a Cl-deficient taseqite variety ("monochlore taseqite"), which differs from "dichlorotaseqite" (found only in the Ilimaussaq massif) by a lower amount of chlorine.

Keywords: eudialyte group; taseqite; Odikhincha massif; alkaline massif; pegmatite; postmagmatic process

Citation: Zaitsev, V.A.; Chukanov, N.V.; Aksenov, S.M. Chlorine-Deficient Analog of Taseqite from Odikhincha Massif (Russia): Genesis and Relation with Other Sr-Rich Eudialyte-Group Minerals. *Minerals* **2022**, *12*, 1015. https://doi.org/10.3390/min12081015

Academic Editor: Paola Bonazzi

Received: 14 May 2022
Accepted: 4 August 2022
Published: 12 August 2022

1. Introduction

The eudialyte group combines 31 mineral species approved by the Commission on New Minerals, Nomenclature and Classification of the International Mineralogical Association (CNMNC IMA). This group is unique due to wide variations of chemical composition, different schemes of isomorphous substitutions and unique structural features. The general formula of eudialyte-group minerals (EGMs) is $\{N(1)_3N(2)_3N(3)_3N(4)_3N(5)_3\}[M(1)_6M(2)_3M(3)M(4)Z_3[Si_{24}O_{72}]Ø_{0\text{-}6}\}X(1)X(2)$, where N(1–5) = Na, H_3O^+, K, Sr, *REE*, Y, Ba, Mn, Ca, □; M(1) = Ca, Mn, *REE*, Na, Fe; M(2) = $^{IV,V}Fe^{2+}$, $^{V,VI}Fe^{3+}$, $^{V,VI}Mn^{2+}$, $^{V,VI}Na^{+}$, $^{IV,V}Zr^{4+}$; M(3) and M(4) = ^{IV}Si, ^{VI}Nb, ^{VI}Ti, $^{VI}W^{6+}$, □; Z = Zr, Ti, Nb; Ø = O, (OH); X = Cl, F, S^{2-}, H_2O, CO_3 and SO_4. In EGMs, more than 14 components can be species defining, including high-field-strength elements (Zr, Ti, Nb, W), large cations (Na, K, Ca, Sr, *REE*) and volatile components (CO_3^{2-}, S^{2-}, H_3O^+, SO_4^{2-}, H_2O and Cl^-) [1–5]. Considerable amounts of *REE*, Zr and Nb make EMGs a prospective source for these critical metals.

Due to variability of structure features and chemical composition, EGMs are considered as perspective indicators of the conditions of petrogenetic processes. Moreover, EGMs play an important role in the balance of volatile components, i.e., it was previously shown by Eggenkamp et al. [6] that EGMs as well as sodalite-group minerals accumulate most of Cl^- and Br^- of agpaitic rocks. Eggenkamp et al. [6] also showed that the distribution coefficients of halogens and sulfur between EGM and feldspathoid significantly vary. However,

the lack of thermodynamic data and information about the mutual influence of components make it difficult to reconstruct directly the physicochemical conditions, such as temperature, pressure, melt composition and oxygen fugacity [7]. Thus, to understand better the relationship between isomorphism, distribution of elements over different crystallographic sites and find the relationship with the geochemical processes, it is necessary to study the eudialyte-group minerals and collect as many cases as possible.

EGMs play a role of accessory and even rock-forming components in peralkaline silica-saturated [8] and silica-undersaturated agpaitic rocks. EGMs are generally found in massifs of agpaitic nepheline syenites, such as Khibiny, Lovozero, Ilimaussaq [9], etc., and much rarely, EGM-bearing rocks may be found in alkaline-ultramafic massifs, such as Konder [10] and Inagli [11], and extremely rarely, in typical alkaline-ultramafic massifs with carbonatites, such as Kovdor [12] or Salpeterkop [13]. In this paper, we report the mineralogical features of EGM found in the pegmatite of the Odikhincha massif, a typical alkaline-ultramafic-carbonatite massif.

2. Geological Setting

Odikhincha is the second largest alkaline complex of the Maymecha-Kotuysky alkaline-ultramafic magmatic province (57 km^2), located at the northwest slope of the Anabar anticline. Geographically it corresponds to the Odikhincha mountain, situated in the Polar Siberia in the Taymyrsky Dolgano-Nenetsky administrative District of Krasnoyarsk Krai, Russia, 588 km east from Norilsk city and 120 km south of Khatanga settlement (Figure 1).

Figure 1. Location of Odichincha massif on the landscape image.

The alkaline rocks of the Odikhincha massif intrude Cambrian and the underlying Riphean dolomites and silicified dolomites. The massif was formed by compositionally contrasting, consistently created intrusions (intrusive phases) of olivinites, melilitic rocks, jakupirangite-melteigites, ijolite-urtites and ijolite-melteigites (Figure 2). Olivinites present in xenoliths among ijolites and melteigites up to 2 × 1 km in the plan. Melilite rocks (melilitolites, turjaites, okaites and uncompahgrites) form a sickle-shaped body 9 × 0.5 km in the eastern part of the massif and also compose outlier blocks among the ijolites in the north of the massif up to 1 × 2 km. Melteigites and jacupirangites form a half-circular subvertical intrusion in the northern, eastern and southern margins of the massif; they also present as xenolites among ijolites. Ijolites, ijolite-melteigites and ijolite-urtites compose a stock 6.3 × 6.6 km, occupying the central and southwestern parts of the massif. The dikes and veins of the ijolites cut through and metamorphose the rocks of all earlier intrusive phases. The areas occupied by the rocks in the main intrusive phases at the current level of exposure are 1.4, 5.7, 12.6 and 37.3 km^2, respectively. Calcite carbonatites and agpaitic

nepheline-syenite-pegmatites form rare dykes, which cut ijolites and other rocks of the massif [14,15]. The presence of carbonatites only in the form of dykes is a unique feature of Odikhincha compared to another massif of the Maimecha-Kotuy province [15], evidencing a relatively big erosion of the massif [16].

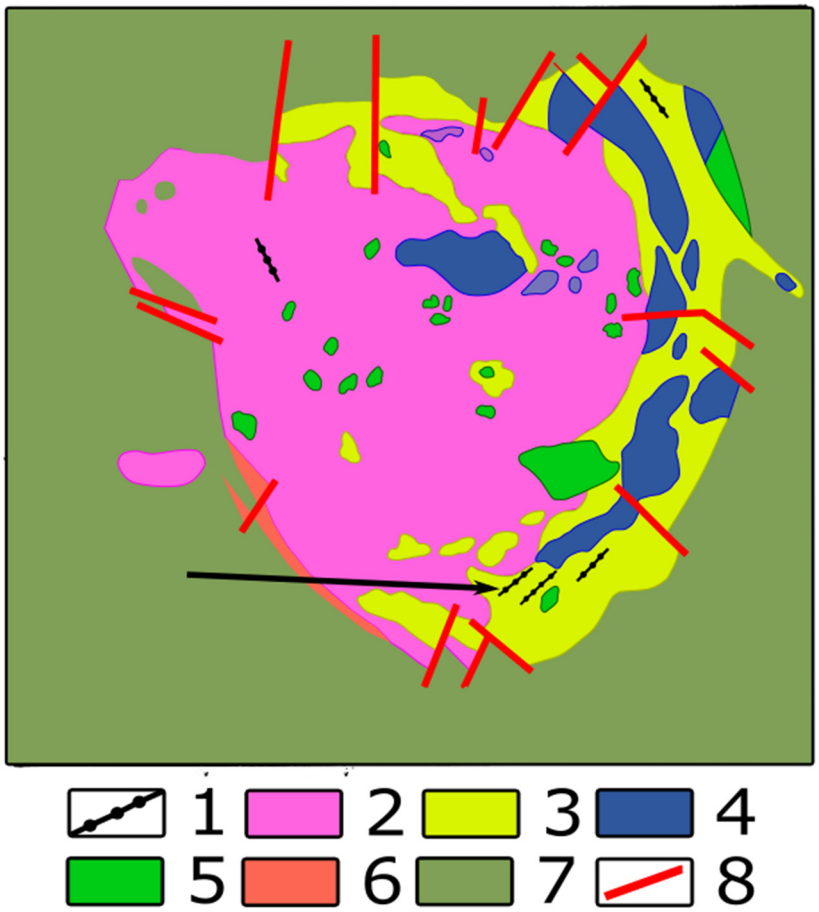

Figure 2. Geological map of Odikhincha massif (simplified from Ref [14]). 1—vines of nepeline-syenite pegmates; 2—ijolites, including melanite ijolites, melaijolites and felspatized melaijolites; 3—melteigites and jacupirangites; 4—melelite rocks; 5—olivinite xenolites; 6—dolerites; 7—Cambrian and Precambrian sedimentary carbonate rocks; 8—faults. The black arrow indicates the sampling point.

The age of the Odikhincha massif was estimated by the U-Pb SHRIMP II method using the perovskite from ijolite (266 ± 3 Ma) and from olivinite (259 ± 6.5 Ma) [15] by the ID-TIMS method using a titanium-bearing andradite from the alkaline pegmatoids, which comprise nepheline, garnet, diopside, phlogopite and apatite as 250 ± 1 Ma [17]. The Rb-Sr isochrone dating shows significant variations in the isochrones' slope (corresponding to 212–240 Ma), which assumed to reflect a contamination by the Sr-rich brain, genetically connected with the interaction between alkaline magma and the surrounding rock in the contact zones of intrusion [18]. Calcite carbonatite from the outcrop in the Ebe-Yuryakh stream was dated by the Rb-Sr isochrone method (258.04 Ma), U-Pb ay apatite (272 ± 27 Ma), Ar/Ar stepwise heating method on mica (264.3 ± 3.0 Ma) and apatite fission-track method (185.0 ± 11.7) [19]. The last data was interpreted as the evidence that after the emplacement at the near-surface depths at about 250, the Ma complex was then buried below the 110 °C isotherm due to significant volcano-sedimentary cover accumulation.

The 3.5 m thick peralkaline nepheline-syenite pegmatite, opened with a trench in the southern part of the massif on the left coast of temporary inflow of the Ebe-Yuryakh stream (70°53′46″ N 103°7′54″ E) near the outcrop of calcite carbonatite with apatite, phlogopite,

magnetite and minor chalcopyrite (used for isotope and fission-track dating, see Ref [19]), was found during the field work. The studied pegmatite is located at 70 m NE from the small pegmatite vein, a type locality of odikhinchaite [20]. However, despite the close location of the two pegmatites within the Odikhincha massif, their mineral compositions are significantly different. The thin pegmatite vein is composed of coarse-crystalline orthoclase, albite, aegirine, cancrinite and subordinate odikhinchaite and ancylite-(Ce). The thick pegmatite is composed of two contrast zones:

- fine-grained aggregate of nepheline, feldspar, aegirine and wollastonite with poikilitic crystals of lamprophyllite and flakes of rinkite-group minerals;
- coarse-crystalline zone, with tabular crystals of a brown Sr-rich eudialyte-group mineral, and gray plates of the K-Na feldspar surrounded by the aggregate, consist of cancrinite crystals, idiomorphic against zeolite and streaks of interstitial brown mass of rinkite-group minerals. Cancrinite crystals contain irregular inclusions of nepheline. The bronze-color lamprophyllite blades and black needles of pyroxene are disseminated in light mass or gathered in spherules (Figure 3).

Figure 3. The sample of Odikhincha peralkaline pegmatite (17 × 14 cm). Coarse-graine part: EGM—reddish-brown, orthoclase—gray, nepheline and hydroxycancrinite mass—pale yellow, aegirine—black, fine-graine aggregates—dark-gray.

Such difference in the mineralogical composition of pegmatites can, probably, explain that the odikhinchaite-bearing pegmatite is located among fine-grained melteigites, while the pegmatite under study—near the contact of melteigites with calcite carbonatite.

3. Methods

3.1. Electron Probe Microanalysis

Electron probe microanalysis of EGMs was performed in the Vernadsky Institute of Geochemistry and Analytical Chemistry, Russian Academy of Sciences on an SX 100 X-ray spectroscopy microanalyzer (Cameca, Gennevilliers, France), equipped with four crystal-diffraction spectrometers; the electron accelerating voltage was 15 kV, and the probe current was 30 nA. Samples were coated with carbon by vacuum evaporation. To reduce the migration of elements to a minimum, the analysis was performed by a defocused probe of 20 μm in diameter, in a fixed order of elemental identification (with Na and Si identified first). The standards and X-ray lines used were as follows: jadeite

(Na Kα, Al Kα, Si Kα); augite (Ca Kα); rhodonite (Mn Kα); zircon (Zr Lα); Cs_2Nb_4O11 (Nb Lα); ilmenite (Ti Kα, Fe augite); metallic Hf (Hf, Mα); orthoclase (K, Si); barite (S Kα); celestine (Sr Lα); vanadinite (Cl Kα); synthetic phosphates of Ce, La, Nd, Y (all Lα). The detection limits were (in mass %): Na—0.02; Al—0.01; Si—0.02; S—0.05; Cl—0.05; K—0.03; Ca—0.03; Ti—0.04; Mn—0.08; Fe—0.07; Sr—0.20; Y—0.20; Zr—0.15; Nb—0.15; La—0.14; Ce—0.18; Hf—0.18. The chemical composition of the associated minerals was studied in the Vernadsky Institute of Geochemistry and Analytical Chemistry, Russian Academy of Sciences using the TESCAN MIRA 3 electron microscope with X-Max Oxford EDS detector. The standards and X-ray lines used were as follows: albite (Na, Kα), Al_2O_3 (Al Kα), SiO_2 (Si, Kα); KBr (K), wollastonite (Ca Kα); Ti (Ti, Kα) Mn (Mn Kα); Fe (Fe Kα); MgO (Mg Kα), zircon (Zr Lα); Nb (Nb Lα); BaF_2 (Ba Lα); LaB_6 (La Lα); CeO_2 (Ce Lα); Nd (Nd Lα); ThO_2 (Th Mα).

The H_2O content was determined by the Alimarin method to be 0.90 wt.%; this value, recalculated for 25.41 Si atoms, yields 3.17 hydrogen atoms.

3.2. Infrared Spectroscopy

Infrared (IR) absorption spectra were recorded in the Institute of Problems of Chemical Physics Russian Academy of Sciences Chernogolovka, Russia on an ALPHA FTIR Fourier spectrometer (Bruker Optics, Ettlingen, Germany) with a resolution of 4 cm^{-1}; the number of scans was 16. Mineral powder was preliminarily pressed into a pellet with anhydrous KBr; a similar pure KBr pellet was used as a comparison sample.

The attenuated total reflectance spectra were recorded in a spectral range of 4000 cm^{-1} to 600 cm^{-1} with an ALPHA II FTIR Spectrometer with Eco-ATR single reflection module equipped with 100 mkm diameter Ge ATR crystal (Bruker Optics, Ettlingen, Germany), located on the Moscow office of Bruker Optics Ltd. A total of 24 scans were averaged for each spectrum with a spectral resolution of 4 cm^{-1}. The Kramers–Kronig transformation was performed by the OPUS 6.0 software (Bruker Optik GmbH, Ettlingen, Germany).

3.3. X-ray Diffraction

The results of the X-ray diffraction study of this material were published earlier [21].

4. Results

4.1. General Features of Studied Pegmatite

As was mentioned above, the studied pegmatite is composed of two contrast zones that differ in texture and mineral assemblages: lujavrite-like zone and coarse-crystalline zone, respectively. The lujavrite-like zone consists of a fine-grained nepheline-pyroxene aggregate, where elongated nepheline grains up to 300 × 500 μm are bypassed by "streams" of subparallel-oriented crystals of clinopyroxene up to 20 × 500 μm in size and surrounded by fine-grained potassium feldspar, cancrinite and analcime. Some of nepheline crystals are monocrystals, but most of them consist of four–five crystals with a typical granoblastic relationship. The zone also contains poikilitic crystals of zonal pyroxene-II (up to 300 × 1000 mkm) and lamprophyllite (up to 200 × 150 μm), irregularly distributed by xenomorphic grains of potassium feldspar (up to 1 mm), pectolite and Sr-rich apatite mineral, as well as rinkite-like mineral (up to 800 μm lumpy spherulites). Potassium feldspar contains inclusions of pectolite, halena, djerfisherite and maucherite (?); it is intersected by thin veins of albite. Polyphase inclusion with tetraferriphlogopite, Na-zeolite and Sr-rich burbankite-group carbonate was found in nepheline.

A coarse-grained zone is composed of gray lamellar crystals of K-feldspar up to 3 × 0.5 cm in size, tablet crystals of EGMs up to 1.5 × 1.5 × 0.5 cm and clinopyroxene spherulites containing xenomorphic EGMs grains in the central part, submerged in a grayish-yellow mass, where cancrinite with nepheline inclusions, is idiomorphic to an aggregate of rinkite-group minerals. This mass is crosscut by zeolite veinlets. The needle-like black crystals of clinopyroxene and bronze plates lamprophyllite are disseminated in the mass of nepheline and cancrinite.

Nepheline is abundant in both zones of pegmatite. In the fine-grained zone it forms isometric crystals, idiomorphic against other minerals; in the coarse-grained zone, it presents as inclusions in crystals of cancrinite. Nepheline composition is given in Table 1. The low analytical total reflects the instability of nepheline during the microprobe analysis. Inside the nepheline, clinopyroxene crystals and polyphase inclusion with phlogopite with an empirical formula $(K_{0.96}Na_{0.03})(Mg_{1.97}Fe_{0.94}Mn_{0.06}Ti_{0.03})[Al_{0.96}Si_{3.05}O_{10}](F_{0.16}OH_{1.84})$ and burbankite with empirical formula $Na_{1.89}K_{0.13}Ca_{1.28}Fe_{0.07}Sr_{2.50}Ba_{0.06}La_{0.03}Ce_{0.04}(CO_3)_{5.02}$ were found.

Table 1. Chemical composition (wt.%) of nepheline and feldspar.

	Fine-Grained Zone				Coarse-Grained Zone		
	Nepheline	**Orthoclase**	**Ba-Rich Orthoclase**	**Albite**	**Nepheline**	**Na-Rich Orthoclase**	**Na-Poor Orthoclase**
n	4	6	1	1	3	7	5
SiO_2	41.54	64.14	61.30	69.89	42.41	65.68	65.07
Al_2O_3	32.15	17.73	18.05	19.22	33.12	18.20	18.16
Fe_2O_3	0.86	0.28	0.52	0.00	0.69	0.27	0.07
Na_2O	14.79	0.91	0.94	9.78	15.91	0.99	0.20
CaO	b.d.l.	0.06	b.d.l.	b.d.l.	n.a.	0.01	0.05
K_2O	6.82	14.91	14.08	0.20	7.00	15.12	16.44
BaO	n.a.	0.71	3.11	0.00	n.a.	0.51	0.52
SrO	b.d.l.	b.d.l.	n.a.	0.60	n.a.	0.03	0.07
Total	96.15	98.73	98.00	99.69	99.14	100.81	100.59

b.d.l.—below the detection limit.

Cancrinite forms elongated crystals up to 2 × 1.5 mm, with inclusions of nepheline, rinkite minerals and pyroxene crystals. The feature of the mineral is low calcium (1.5–2 wt.% CaO) and high Sr (1.5–3 wt.% SrO) content. The identification of the mineral was confirmed by IR and Raman spectra.

Feldspars. Orthoclase is one of the most conspicuous minerals. In the coarse-grained zone, it forms bluish gray plate-shape idiomorphic crystals, surrounded by the late minerals, including cancrinite, pyroxene and titanite. Na-poor orthoclase was found together with analcime in the secondary solid inclusions in EGMs crystals. In the lujavrite-like zone, orthoclase was found as part of the fine-grained hypidiomorphic mass and elongated grains with inclusions of nepheline, pyroxene and sulfides. The thin veins of albite crosscut these crystals. The chemical composition of feldspar minerals is shown in Table 2. The majority of orthoclase from both zones contains ~1 wt.% of Na_2O and ~0.3 wt.% of Fe_2O_3, while some analyses of orthoclase show significantly lower concentrations of these elements.

Table 2. Chemical composition (wt.%) of clinopyroxene.

	Fine-Grained Zone		Coarse-Grained Zone	Inclusions in Eudialyte
	Yellowish-Green to Green	**Green to Blueish-Green**		
Na_2O	6.73–8.53	9.42–9.69	7.38–11.31	8.52–9.38
MgO	1.57–4.32	0.91–2.03	1.35–4.95	1.57–1.99
Al_2O_3	0.66–1.02	0.68–1.11	0.58–0.99	0.66–0.85
SiO_2	50.30–51.79	51.15–51.61	51.64–54.32	50.80–51.64
CaO	7.13–11.17	5.60–6.06	4.01–10.54	6.11–7.13
TiO_2	0.92–1.82	1.10–1.38	1.02–4.05	1.00–1.02
MnO	0.44–0.69	0.45–0.61	0.52–1.37	0.52–0.69
FeO	20.70–25.43	24.24–26.85	18.30–26.74	24.91–25.43
Total	94.99–97.79	96.21–96.78	96.42–101.25	95.80–96.42

Clinopyroxene is the predominant mineral in the fine-grained zone and a minor mineral in the coarse-grained zone. Clinopyroxene is represented by the diopside-hedenbergite-aegirine solid solution (Table 2). Tetrahedral sites are fully occupied by Si. Ti content is

variable, reaching 4 wt.% TiO_2 in cores of zoned crystals from the coarse-grained zone. Due to the absence of Al in the tetrahedral sites, the only Ti-aegirine mechanism of the substitution can accommodate tetravalent cations in the *M*(1) site in clinopyroxene (Ti-aegirine end-member formula is $NaTi_{1/2}Fe^{2+}{}_{1/2}Si_2O_6$ [22]). There are two varieties of clinopyroxene in the fine-grained zone: pyroxene-I with yellowish-green to green pleochroism and pyroxene-II with slight pleochroism from green to blueish-green. Both varieties form an unevenly grained aggregate of disordered crystals up to 150 × 30 μm, but pyroxene-II also forms crystals up to 0.3 × 2 mm in size with poikilitic inclusions of nepheline, feldspar and pectolite.

The chemical composition of pyroxene shows a continuous trend (Figure 4). The clinopyroxene from pegmatite sharply differs from the pyroxene of the early phases of the Odikhincha intrusion formation, in that it has a significantly lower content of the diopside and a higher content of the aegirine component.

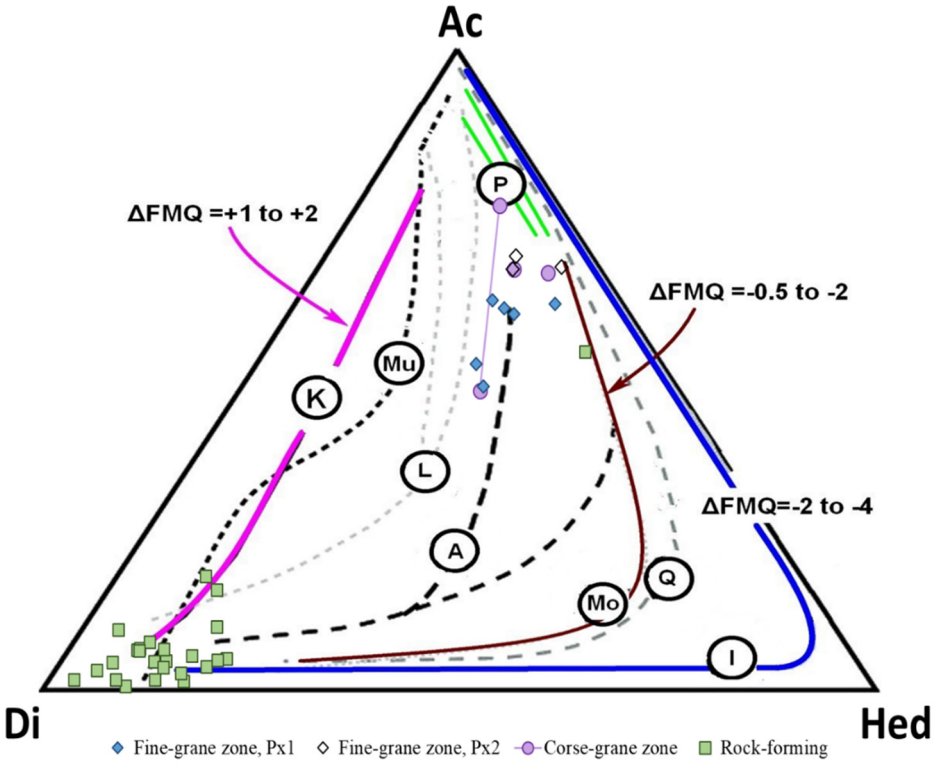

Figure 4. Composition of clinopyroxene from Odikhincha intrusion: our data for clinopyroxene from pegmatite and for rock-forming clinopyroxene (data from Ref [23]) in terms of Di-Hed-Ac (Mg–(Fe^{2+} + Mn)–Na) in comparison with evolution trends of various alkaline complexes: (K) Katzenbuckel, SW Germany (Mu) Murun, Siberia, (L) Lovozero, Kola Peninsula, (A) Alnö, Sweden (Mo) Motzfeldt, South Greenland, (Q) North Qôroq, South Greenland, North Qôroq, South Greenland) (I) Ilímaussaq. P- Pilansberg [24–27] Quantitative data on oxygen fugacity (given as ΔFMQ units, where FMQ is the fayalite-magnetite-quartz buffer) for Katzenbuckel, Ilímaussaq and Motzfeldt are given from Refs [24,27,28].

Pectiolite is abundant in the fine-grained zone; it forms syngenetic epistaxis inclusions in clinopyroxene-II and also xenomorphic grains, with inclusions of pyroxene-I.

Lamprophyllite forms bronze-yellow needle-shape crystals up to 1 mm long. The chemical composition of lamprophyllite is shown in Table 3. The compositions of lamprophyllite in both zones of pegmatite are similar and may be subscribed by the empirical formula $(Sr_{1.32}Na_{0.49}K_{0.11}Ba_{0.09})$ $(Na_{2.13}Ca_{0.15}Mg_{0.10}Mn_{0.20}Fe_{0.31}Ti_{2.86}Nb_{0.01})Si_{4.00}$ … $F_{0.78}$. This composition is notable by the low potassium, barium and manganese content relative

to the worldwide lamprophyllite variations [29]. Polyphase inclusion with nepheline, sodalite and Sr-Ba-carbonate was found in lamprophyllite from the fine-grained zone.

Table 3. Chemical composition (wt.%) of lamprophyllite, rinkite-group minerals and titanite associated with EGMs in peralkaline pegmatite of Odikhincha massif.

	Lamprophyllite		Rinkite-Group Minerals			Titanite
			Rinkite-(Ce)	Mosandrite-(Ce)	Unnamed Mineral	
n	4	1	5	3	7	2
SiO_2	30.11	31.55	29.34	25.15	34.43	28.84
TiO_2	28.67	29.68	7.66	9.62	12.88	38.33
Al_2O_3			0.09	0.35	5.19	0.21
FeO	2.80	2.97	0.05	0.22	0.59	1.97
MnO	1.77	1.66				0.01
MgO	0.51	0.40				
CaO	1.09	0.78	26.38	21.01	4.09	26.38
SrO	17.30	17.36	5.94	2.51	1.55	0.92
BaO	1.60	2.21				
K_2O	0.65	0.67		0.30	0.51	0.01
Na_2O	10.13	10.87	6.34	0.70	0.16	0.76
Nb_2O_5	0.23	0.24	3.59	2.53	5.22	1.52
ZrO_2			0.09	0.39		0.06
La_2O_3			4.71	4.79	7.17	0.21
Ce_2O_3			5.38	9.18	9.72	0.50
Nd_2O_3			0.72	0.78	1.06	
Y_2O_3			0.35	0.74	0.33	
ThO_2			1.21	1.85	2.34	
UO_3			0.39	0.53	0.36	
F	1.83	2.03	6.75	1.50	0.00	
Total	94.86	98.39	92.23	80.65	85.60	99.69

Titanite forms rare crystals, both in fine-grained and in coarse-grained zones. In the fine-grained zone, titanite associated with lamprophyllite, and in the coarse-grained zone, idiomorphic titanite was included into cancrinite.

Three rinkite-group minerals, identified from the microprobe analyses (Table 3), were found: rinkite-Ce with empirical formula $Ca_{3.85}Na_{1.67}REE_{0.55}Sr_{0.47}Ti_{0.78}Nb_{0.22}(Si_2O_7)_2F_{2.91}$, mosandrite-(Ce) $Ca_{3.60}REE_{0.90}Sr_{0.22}Na_{0.20}Ti_{1.15}Nb_{0.18}(Si_{2.97}Al_{0.03})_2F_{0.66}$ … and unnamed cation-deficient mineral with the formula $Ca_{0.43}Na_{0.03}Sr_{0.08}REE_{0.66}Ti_{0.96}Nb_{0.23}Si_{3.40}Al_{0.60}F_{0.00}$. **Rinkite-(Ce)** forms thin, up to 0.3 mm long crystals in both zones of pegmatite. The crystals may be scattered or segregated in felt-like aggregates. In the fine-grained zone, these aggregates overlay the pattern of rock-forming minerals; in the coarse-grained zone, these aggregates surround the crystals of Na-zeolite with rinkite inclusions. Other rinkite-group minerals substitute rinkite crystals. Small loparite crystals (up to 10 mkm) were found in association with rinkite. The low analytical sum of rinkite-like mineral is connected with high H_2O content.

4.2. Morphology, General Physical and Optical Properties of EGMs

EGMs form nicely shaped flattened crystals up to 1.5 × 1.5 × 0.5 cm in size. The crystals show combinations of pedions with triangular shading prisms and trigonal pyramids. The crystals are dark reddish-brown. Thin (<1 mm) splinters of crystals are brown as buckwheat honey, with vitreous luster. The streak is white. No cathodoluminescence or fluorescence were found under short- and long-wave ultraviolet light, but strong laser-inducted luminescence was observed during Raman spectroscopy experiments. The mineral is brittle, with uneven fracture; the cleavage parallel to the pinacoid was observed only in polished preparates' fracture direction, as well as fracture direction parallel to the pyramid and prism faces. The Mohs hardness is 5.

The crystals consist of a core and shell and differ in the zoning type: the core of the crystals shows spotted zoning in composition, while the shell shows clear oscillatory zoning with micrometer range and often contains inclusions of pyroxene and rinkite-like mineral (Figure 5). The border between the core and the rim zones has irregular, smooth shape (see Figure 5b,c), which obviously evidences the dissolution event. In contrast with the core, the shell contains aegirine crystals and polyphase inclusions filled by orthoclase and zeolites. The secondary taseqite forms thin veinlets, crosscutting both the core and the shell of the primary taseqite crystals. Sometimes, the central part of such veinlets is filled by zeolites. In the fine-grained zone, the EGMs form xenomorphic to amoeba-shaped irregular poikilitic crystals, surrounding the nepheline and pyroxene.

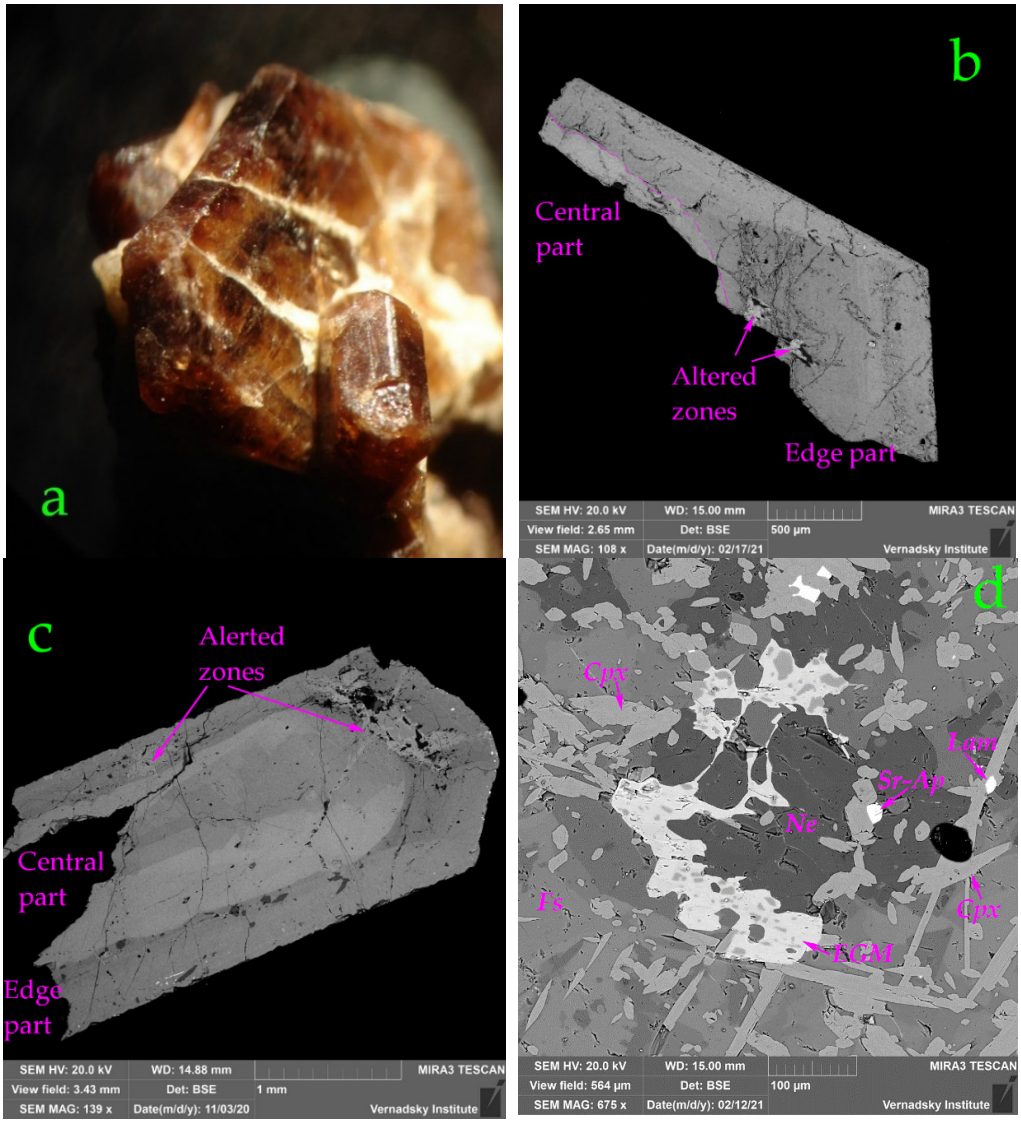

Figure 5. Optical photo (**a**) and BSE images of EGMs crystals (**b**–**d**).

4.3. Chemical Composition of EGMs

The chemical data for EGMs are given in Table 4. The contents of the elements with the atomic numbers <8 are below detection limits. The formula coefficients were calculated following Ref [1], based on the sum of (Si + Zr + Ti + Nb + Al + Hf) cations normalized to 29 cations per formula unit (p.f.u.), and the portions of all others were multiplied to this standardization. Si and Al are summed, and excess Si to 24 a.p.f.u. (atoms per formula unit) is added to *M*(3) and *M*(4) sites. All Zr and Hf are assigned to the Z site, and the

deficiency in this position is filled up to 3 a.p.f.u. by Ti; the remaining Ti is assigned to the *M*(3) site together with Nb and Si. Fe and Mn are allocated to the *M*(2) site, and the small deficiency makes up the total to three atoms with Na, based on the generalization of the structured data [5]. Based on the X-ray absorption spectroscopy results [30], all lanthanides are assigned to the *M*(1) site together with Ca. The excess of Ca are assigned to the *N* sites together with elements with large ionic radii. The calculated coefficients are given in Table 5. In accordance with the classification of EGMs, the studied sample is taseqite.

Table 4. Chemical composition (wt.%) of EGMs from Odikhincha massif.

Constituent	Well-Shaped Euhedral Crystal						Xenomorphic	
	Central Part		Edge Part		Alerted Zone			
	Mean	Range	Mean	Range	Mean	Range	Mean	Range
Na_2O	11.63	10.81–12.16	11.49	9.94–12.53	10.48	9.27–11.43	10.04	8.32–11.43
K_2O	0.65	0.4–0.79	0.62	0.42–0.74	0.67	0.61–0.74	0.27	0.22–0.37
CaO	11.13	10.56–12.07	11.38	10.47–11.88	11.45	11.14–12.08	11.25	11.08–11.42
SrO	5.20	3.82–6.37	4.96	3.94–5.7	5.91	5.02–6.84	4.75	3.82–5.39
BaO	0.10	0.1–0.1	0.04	0.04–0.04	0.35	0.35–0.35		
Y_2O_3	0.01	0–0.05	0.01	0–0.03	0.02	0–0.11		
La_2O_3	0.27	0.1–0.55	0.20	0.04–0.47	0.47	0–0.87	0.14	0.09–0.19
Ce_2O_3	0.26	0–0.54	0.24	0.06–0.48	0.43	0.09–0.83	0.27	0.24–0.29
Nd_2O_3	0.04	0.04–0.06	0.06	0–0.11	0.08	0.08–0.08	0.04	0–0.12
MnO	1.46	1.06–2.17	1.61	0.37–2.07	1.77	0.45–2.47	1.86	1.73–2.04
FeO	4.99	4.71–5.36	4.80	4.22–5.35	4.16	3.74–4.61	5.12	4.91–5.49
TiO_2	0.76	0.4–1.63	0.98	0.43–1.78	0.40	0.22–0.57	0.89	0.68–1.27
Nb_2O_5	2.37	1.56–3.61	2.34	1.81–3.13	3.01	2.21–3.68	2.22	2.03–2.36
ZrO_2	11.14	9.36–11.94	10.56	9.53–11.73	11.50	10.46–12.42	10.14	9.66–10.97
HfO_2	0.13	0.09–0.17	0.08	0–0.13	0.19	0.15–0.25	0.12	0.08–0.17
SiO_2	48.49	45.3–51.09	49.36	47.39–52.03	47.58	44.96–49.62	49.02	48.45–49.48
SO_3	0.17	0.08–0.24	0.18	0–0.27	0.14	0.06–0.23		
Cl	0.96	0.8–1.08	0.95	0.81–1.05	0.67	0.49–0.93	0.77	0.74–0.8
Total	99.53	97.27–101.93	99.71	95.71–102.66	98.71	94.98–102.82	96.89	95.86–97.64

Table 5. Empirical formula coefficients for EGMs from Odikhincha massif.

		Central Part		Edge Part		Alerted Zone		Xenomorphic	
N sites	Na	11.60	10.85–12.21	11.23	9.78–12.32	10.74	9.43–11.87	10.13	8.44–11.50
	Ca	0.32	0.00–0.60	0.36	0.00–0.58	0.66	0.40–1.00	0.36	0.24–0.51
	Sr	1.57	1.10–2.03	1.48	1.21–1.71	1.81	1.50–2.09	1.43	1.15–1.64
	K	0.43	0.26–0.53	0.41	0.28–0.48	0.45	0.39–0.51	0.18	0.15–0.24
M(1) site	Ca	5.90	5.79–5.96	5.92	5.82–5.97	5.83	5.68–5.97	5.92	5.90–5.94
	REE	0.10	0.04–0.21	0.08	0.03–0.18	0.17	0.03–0.32	0.08	0.06–0.10
M(2) site	Fe	2.17	2.01–2.37	2.07	1.86–2.32	1.84	1.65–2.03	2.23	2.15–2.39
	Mn	0.66	0.46–0.95	0.69	0.00–0.90	0.73	0.00–1.09	0.82	0.77–0.90
	Na	0.17	0.00–0.36	0.24	0.01–0.83	0.43	0.14–1.17	0.03	0.00–0.08
M(3,4)sites	Nb	0.57	0.36–0.90	0.55	0.42–0.75	0.72	0.51–0.88	0.52	0.48–0.55
	Si	0.31	0.00–0.69	0.42	0.12–0.79	0.17	0.00–0.44	0.54	0.36–0.76
	Ti	0.14	0.00–0.28	0.07	0.00–0.44	0.10	0.00–0.21	0.03	0.00–0.10
Z site	Zr	2.80	2.37–3.00	2.65	2.40–2.88	2.96	2.69–3.15	2.58	2.44–2.80
	Ti	0.19	0.00–0.62	0.35	0.12–0.59	0.06	0.00–0.23	0.31	0.17–0.50
	Hf	0.00	0.00–0.03	0.00	0.00–0.02	0.00	0.00–0.04	0.02	0.01–0.03
X site	Cl	0.85	0.72–0.94	0.83	0.70–0.90	0.60	0.44–0.81	0.68	0.66–0.70

4.4. Infrared Spectroscopy

The Kramers–Kronig-transformed attenuated total reflectance and absorption spectra of Sr-rich EGMs from the Odikhincha alkaline complex are given in Figures 6 and 7. The absorption IR spectrum of taseqite from Odikhincha (curve c in Figure 6 and curve a in Figure 7) includes the following bands (cm^{-1}): 3502, 3326 (O–H stretching vibrations), 1643 w (H–O–H bending vibrations), 1507 w, 1451, 1415 w (asymmetric stretching vibrations of the CO_3^{2-} groups), which are well fixed only in the powder spectra. The strongest absorption diapason of 900–1050 cm^{-1} (Si–O stretching vibrations) includes four bands: the band at 1055 cm^{-1} forms a shoulder in the spectra obtained from the surface, perpendicular to the three-fold axis and absent in the spectra, obtained from the surface, parallel to the three-fold axis. Bands at 1019 and 973 cm^{-1} present in all the spectra, but the intensity of the band at 1019 cm^{-1} varies strongly, while the band at 926 cm^{-1} is strong in the spectra obtained from the surface parallel to the three-fold axis. The intensity of the band at 1019 cm^{-1} in the direction parallel to the three-fold axis obliquely correlated with Nb content, so we can connect it with vibrations of NbO_6 octahedrons in the *M*(3a) site. On the other hand, the intensity of the band at 1019 cm^{-1} inversely correlated with the band at 926 cm^{-1}, corresponding to the additional SiO_4 tetrahedra located at the centers of nine-membered rings [31]. The next area includes bands at 740 cm^{-1} (mixed vibrations of tetrahedral rings—"ring band"), 697 cm^{-1}, 656 cm^{-1} (mixed vibrations of tetrahedral rings combined with Nb–O stretching vibrations). The last two bands show variable intensity, especially in the spectra obtained from the surface, parallel to the three-fold axes. The 542 sh and 528 bands are attributed to the $^{IV}Fe^{2+}$–O and $^{IV}Mn^{2+}$–O stretching vibrations, respectively, 479, 452 (lattice mode involving predominantly bending vibrations of tetrahedral rings), 367 (lattice modes involving Ca–O stretching vibrations). The assignment of IR bands was made based on the analysis of IR spectra of structurally investigated eudialyte-group minerals.

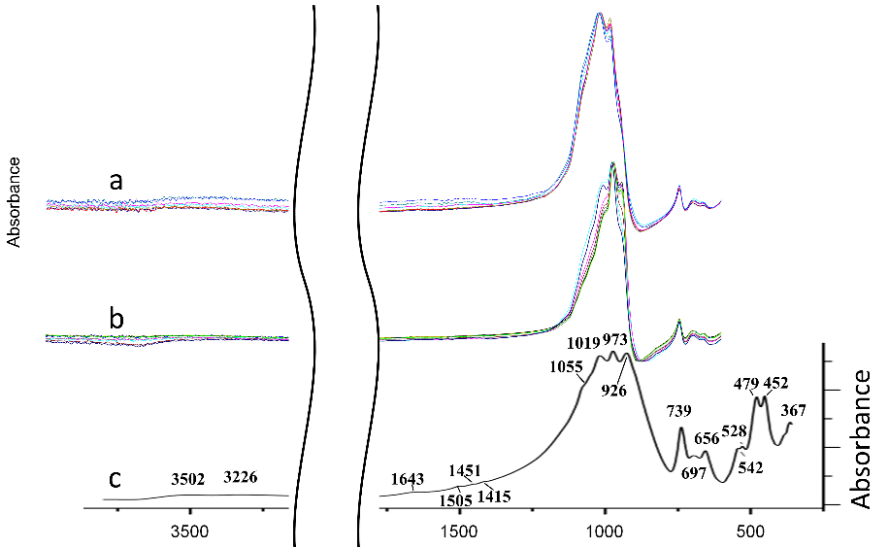

Figure 6. Kramers–Kronig-transformed attenuated total reflectance spectra obtained from the polished surfaces, perpendicular (**a**) and parallel (**b**) to the three-fold axes of the same crystal and powder infrared absorption spectrum of EGMs (**c**) from Odikhincha alkaline complex.

The IR spectra of various Sr- and Nb-dominant EGMs given in Figure 7 are similar. The assignment of IR bands of these minerals was made based on Ref [3]. The ranges of 3300–3600 and 1630–1660 cm^{-1} correspond to O–H stretching and H–O–H bending modes, respectively. The peaks in the range of 1410–1510 cm^{-1} are due to asymmetric vibrations of carbonate groups. Strong bands observed in the regions 920 to 1100, 650 to 670 and 400 to 500 cm^{-1} correspond to Si–O stretching and O–Si–O bending and Si–O–Si bending

vibrations. The distinct peaks near 740 cm^{-1} are related to the mixed vibrations of rings of SiO_4 tetrahedra (so-called "ring band").

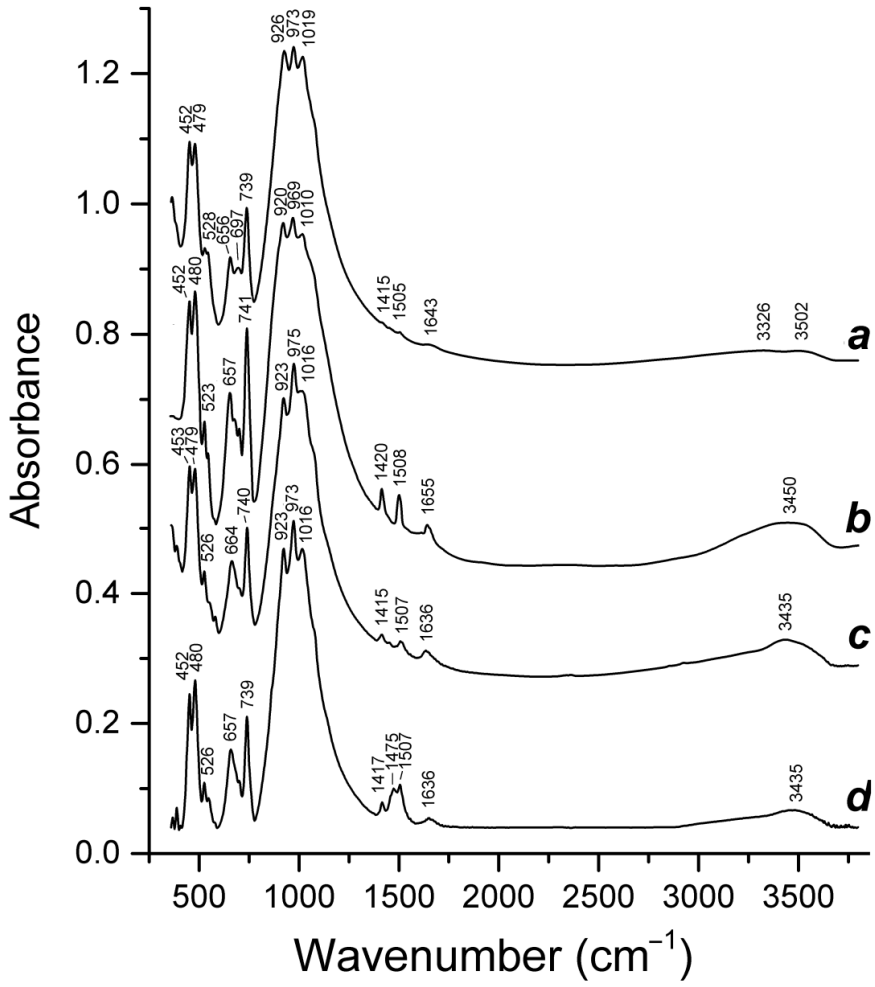

Figure 7. Powder infrared absorption spectra of (**a**) Cl-deficient taseqite from Odikhincha (this work), (**b**) CO_3-bearing Cl-deficient taseqite with the empirical formula $Na_{12.0}(Sr_{1.3}Na_{0.9}K_{0.5}Ca_{0.2}Ba_{0.1})(Ca_{5.7}Mn_{0.3})(Fe_{1.6}Mn_{1.4})Zr_{3.1}Ti_{0.1}Nb_{0.7}Si_{25}O_{73}(O,OH)_xCl_{0.6}(CO_3)_{0.5}{\cdot}nH_2O$ from the Yukspor mountain, Khibiny [32], (**c**) odikhinchaite holotype sample, ideally $Na_9Sr_3[(H_2O)_2Na]Ca_6Mn_3Zr_3NbSi(Si_{24}O_{73})(OH)_3(CO_3){\cdot}H_2O$, from Odikhincha [20] and (**d**) Fe-rich odikhinchaite variety $Na_{11}Sr_3(Mn^{2+},Fe^{2+},Fe^{3+})Ca_6Zr_3Nb[Si_{25}O_{72}(OH)](CO_3)Cl(OH,O)_4$ from the Putelichorr mountain, Khibiny [33].

The band at 526 ± 3 cm^{-1} is a characteristic feature of Mn and Fe occurring at the *M*(2) site and having five-fold coordination (square pyramid). In all IR spectra given in Figure 7, this band has a shoulder between 540 and 550 cm^{-1}, which is an indication of the minor amount of Fe^{2+} with the configuration close to a flat square [3].

In most Cl-deficient Sr- and Nb-dominant EGMs, chlorine is partly substituted by carbonate groups. As seen from Figure 7, taseqite is an exception to this regularity: the bands of CO_3^{2-} groups in its IR spectrum are very weak. Another distinctive feature of this sample is a weak IR band at 3502 cm^{-1}, which may be related to vibrations of OH groups or H_2O molecules at the *X*(2) site.

5. Discussion

The chemical composition of the studied EGMs from the Odikhincha massif is noticeable by the high concentration of Sr and Nb. There are four Sr-dominant eudialyte-group

minerals: khomyakovite, mangankhomyakovite, taseqite and odikhinchaite. The last one is specific due to the predominance of CO_3^{2-} anion in the *X*-site [20]. Sr- and Nb- rich samples of EGMs were also described in Lovozero [34], Khibiny [35] and Pilansberg massifs [36].

The simplified formula of EGMs from Odikhincha based on structure refinement [21] (1) and average EMPA data (2) nominally corresponds to taseqite but differs from the formula of holotype taseqite from Ilimaussak [37], calculated from the structure refinement (3) and chemical data (4):

$$Na_{12}Sr_3Ca_6Fe^{2+}{}_3Zr_3NbSi_{25}O_{72}(OH,O)_4Cl(H_2O)_{0.2}; \quad (1)$$

$$Na_{12}Sr_2Ca_6(Fe,Mn)_3Zr_3(Nb,Ti)Si_{25}O_{72}(OH,O)_4Cl(H_2O)_{0.2}; \quad (2)$$

$$Na1_2Sr_3Ca_6Fe_3Zr_3NbSi_{25}O_{73}(O,OH,H_2O)_3C_{l2}; \quad (3)$$

$$Na_9Sr_5Ca_5Fe_2Mn_2Zr_3NbSiSi_{24}O_{73}(O,OH,H_2O)_3C_{l2}. \quad (4)$$

The distinction can be clearly shown on the Sr vs. Cl and Sr vs. Nb diagrams plot (Figure 8). On the Sr-Nb diagram (Figure 8a), the studied eudialyte, odikhinchaite and Sr-Nb EGMs from the Khibiny, Lovozero and Pilansberg massifs form a single elongated field. One end of this field, where the primary EGMs analyses are located, starts approximately from one-third of the line connecting the points (0; 0) and (1; 3), and the other, where the secondary EGMs points together with points of odikhinchaite and Sr-Nb EGMs from Khibiny, Lovozero and Pilansberg are located, extends toward the point (1; 2). That is, this field has a noticeably lower slope than the line connecting the figurative points of the theoretical composition of eudialyte and most of the minerals of the eudialyte subgroup and the figurative points of the theoretical composition of taseqite and odikhinchaite. Some of the primary EGMs analyses are characterized by the content of niobium and strontium, and chlorine is insufficient to ensure their predominance in the corresponding sites (they may be identified as eudialyte-ss. or labirintite, after additional study), and some of them have insufficient Sr content to be assigned to taseqite but sufficient Nb content to be attributed to ferrokentbrooksite. The holotype taseqite contains 2.47 a.p.f.u. of Sr in the *N*(4) site, 1.1 a.p.f.u. of Sr in the *N*(3) site and 0.3 a.p.f.u. of Sr in the *M*(1) site. It is interesting to note that the sum of strontium is 3.87 a.p.f.u., which is significantly lower than the chemically estimated Sr content (4.84 apfu). The last number may evidence that Sr is dominant not only in the *N*(3) site but also in the *N*(4) site, while «taseqite» from Odikhincha, similar with the «Fe,Sr-analog of kentbrooksite» from Lovozero, contains Sr only in the *N*(4) site.

In the Si-Nb diagram (Figure 8c), the figurative field of the studied EGMs spreads along the line segment, connecting points Si = 26 and Nb = 0, which corresponds to eudialyte-s.s. and others, while Si = 25 and Nb = 1 corresponds to taseqite, odikhinchaite, kentbroksite and others. The figurative points of analyses of xenomorphic grains and idiomorphic crystals are distributed near the half of the section, while the points of secondary EGMs are located toward the Nb-rich side. Primary EGMs (especially in Nb-poor parts) are slightly enriched by Ti both in the *M*(4) and *Z* sites, relative to the secondary one (Figure 8e,f), which might be interpreted as the admixture of labirintite and alluaivite components.

At the Sr vs. Cl diagram (Figure 8b), the figurative points of primary EGMs are located near the point with the coordinates Sr = 1.5 and Cl = 1, which may be described as the mixture of taseqite with kenbrooksite-like end member, as well as the mixture of eudialyte-like end member with odikhinchaite or khomyakovite. The secondary EGM spreads in the direction of odikhinchaite and khomyakovite points. The Na vs. Cl (Figure 8d) diagram also demonstrates that secondary EGMs are slightly poorer in Na than primary ones. These trends show that the late-hydrothermal transformation process results both in enrichment in Sr and leaching of Cl and Na. The EGMs from Khibina, Lovozero and Pilansberg show similar Cl and Na content. In contrast, the taseqite from the Ilimaussak massif is much richer in Cl. There are two chlorine-dominant positions in holotype taseqite but only one in the eudialyte-group mineral from Odikhincha and other Sr-rich EGMs.

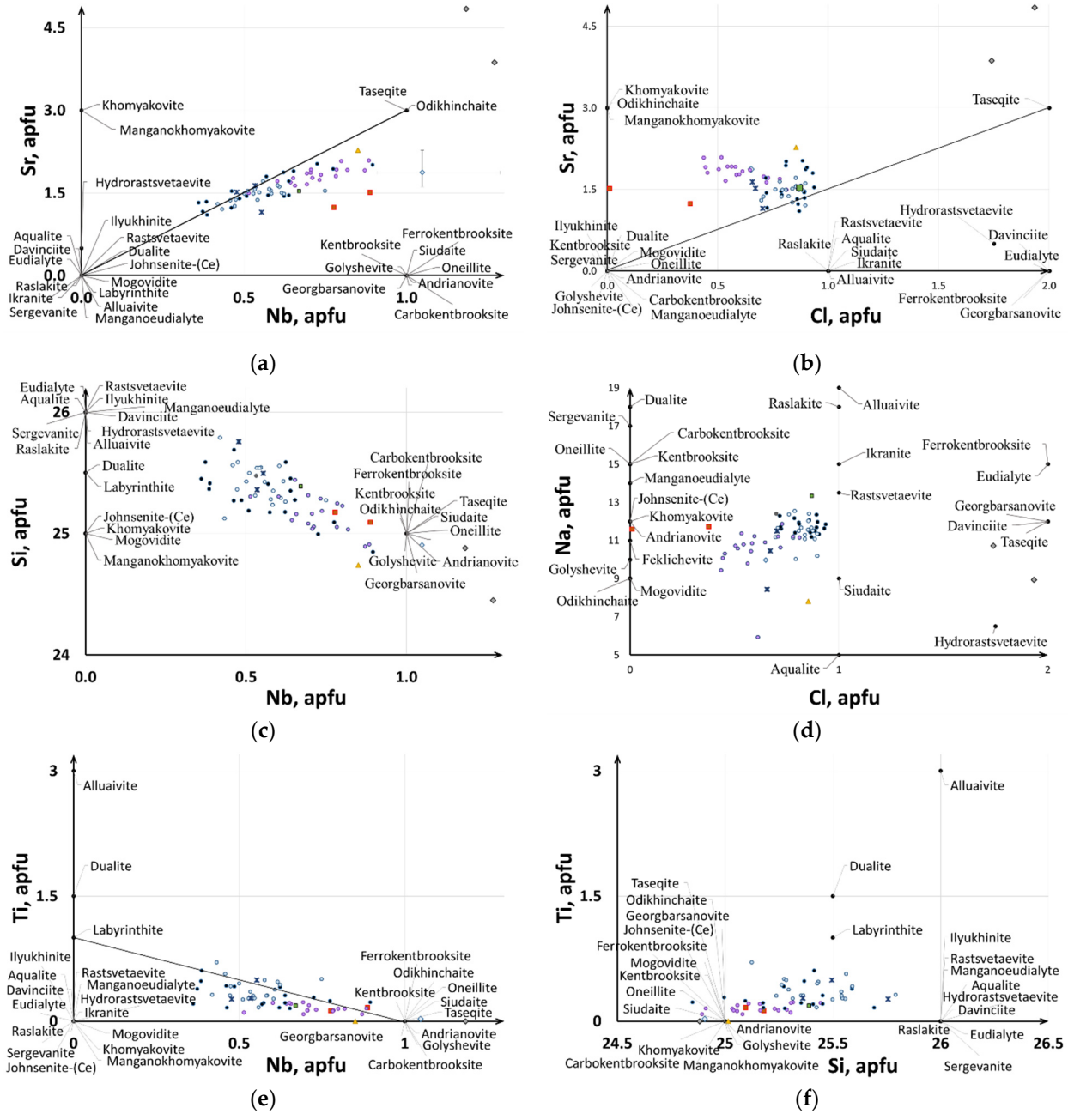

Figure 8. Chemical composition (**a**–**f**) of Nb-Sr-rich eudialyte-group minerals from the Odikhincha massif. New data: dark-blue dots—center and light-blue rime zone; violet dots—secondary zones of idiomorphic crystals; dark-blue crosses—xenomorphic crystals; light-blue diamond—odikhinchaite (Odikhincha); gray diamond—taseqite (Ilimaussak); green square—«Fe,Sr-analog of kentbrooksite (Lovozero)»; red square—«taseqite» (Khibina massif); and yellow triangle—«transitional to taseqite» (Pilansberg) [20,34–37].

Both these features are not enough to establish it as a new mineral species. However, it could be useful to distinguish this variety from the holotype taseqite from Ilimaussak using the prefix «mono-chlore» (Table 6).

Table 6. Site populations (apfu) in the key positions of taseqite and taseqite-like minerals.

Site	«Taseqite», Odikhincha [21]	Taseqite, Ilímaussaq [37]	«Fe,Sr-Analog of Kentbrooksite», Lovozero [34]	Odikhinchaite, Odikhincha [20]
M(1)	5.85 Ca + 0.15 *REE*	4.98 Ca + 0.58 Mn + + 0.3 Sr + 0.14Y	4.85 Ca + 0.85 Mn + 0.30 *REE*	6 Ca
M(2a)	2.43 Fe^{V}	1.25 $Fe^{2+,V}$ + 0.92 Mn^{V}	0.87 $Fe^{2+,IV}$	2.49 Mn + 0.51 Fe
M(2b)	0.45 Mn^{V}	0.68 $Fe^{2+,V}$	1.11 $Fe^{2+,V}$ + 0.67 Mn^{V} + 0.19 Ti^{V} + 0.1Zr^{V} + 0.04 Hf^{V}	
M(3a)	0.64 Nb	0.97 Nb	0.7 Nb + 0.3 Si	Nb
M(3b)	0.33 Si			
M(4a)	0.67 Si	0.3 Nb	Si	0.82 Si
M(4b)	0.27 Ti	0.45 Si		0.18 Si
N(3)	2.5 Na + 0.5 K	1.9 Na + 1.1 Sr	3 Na	2Sr + 0.45 K + 0.2 REE *Ln* 0.35 Na
N(4)	1.71 Sr + 1.29 Na	2.47 Sr + 0.53 Na	1.8 Sr + 0.96 Na + 0.24 K	3 Na
N(5)	3 Na	2.56 Na	3 Na	1.8 H_2O + 1.2 Na
X(1)	0.74 Cl	0.91Cl		0.53 CO_3 + 0.35 Cl 0.12 Cl
X(2)	0.18 H_2O	0.83 Cl		0.6 H_2O 0.4 (OH,F)

Note: The superscripted Roman numerals indicate the coordination number.

The binary diagrams perfectly demonstrate that in spite of the average composition and single-crystal structure refinement data corresponding to the taseqite, part of the analyses of the same crystals should be classified as other mineral species, probably eudialyte and ferrokentbruksite, as they contain less than 1.5 a.p.f.u. of Sr, and therefore, the *N*(4) site is mainly occupied by Na instead of Sr, and the amount of Nb is less than 0.5 a.p.f.u., and therefore, Si predominates in both the *M*(4) and *M*(3) sites, but a crystal structure study is necessary for accurate future identification. The situation is similar for the Sr-Nb minerals of the eudialyte group from the Khibiny, Lovozero and Pilansberg massifs.

The holotype sample of taseqite contains higher contents of niobium, chlorine and strontium relative to the theoretical composition of, taseqite. In the holotype sample, strontium predominates in the *N*(3) site and significantly occupies *N*(4); Nb occupies not only the *M*(3a) site but also *M*(4a); chlorine, as in eudialyte-s.s., fills both the *X*(1) and *X*(2) sites, while in the other Sr-Nb minerals of the eudialyte group, the content of chlorine does not exceed one atom per formula unit, and strontium is not enough to completely fill the *N*(3) site.

Thus, only the Ilimaussak massif mineral can actually be taseqite, while the strontium-niobium minerals from the Odikhincha, Khibiny, Lovozero and Pilansberg massifs constitute a specific variety that can be called "monochlore taseqite".

The mineral assemblage associated with EGMs provides a possibility to estimate the mineral-forming conditions. The composition of nepheline (Figure 9a) corresponds to the formation temperature ~775 °C, which must be attributed to the early pegmatite mineral association. The potassium feldspar composition (Figure 9b) demonstrates a much lower crystallization temperature (300–350 °C) for the main pegmatite mineral association, which includes potassium feldspar, cancrinite, pyroxene-I, pectolite and EGM. Similar temperature estimation follows from the pectolite presence in this association; the experimental data show that pectolite may be synthesized at 300 °C and 80–300 bars and decomposed above 620 °C [38]. The presence of cancrinite also evidences a similar limitation; the proper cancrinite and hydroxyl cancrinite are stable at least up to 800 °C at 1.38 kbar H_2O [39] and up to 930 °C at 2 kbar of H_2O-rich fluid [40]. The Ca-low cancrinite («natrodavyne») transforms to a cubic nosean-type phase at 600–650 °C and 1.38 kbar H_2O [39].

The formation temperature of the late association, which includes the late generation of EGMs and zeolites, is limited to 230 °C because of the presence of chabazite-group minerals.

It was established [24] that the position of clinopyroxene composition trend on the diopside-hedenbergite-aegirine diagram is determined by the oxygen fugacity during the differentiation of the peralkaline system. Practically, we can say that rock-forming clinopyroxene and clinopyroxene from pegmatite are located on the different ends of the Alno differentiation trend, between the trends of Katzenbuckel at ΔFMQ +1–+2 and

Motzfeldt at ΔFMQ −0.5−−2, so we can conclude that the peralkaline system of the Odikhincha pegmatite was formed at the oxygen fugacity near the FMQ buffer (see Figure 4). The presence of the Ti-aegirine component in the clinopyroxene composition is also evident of the low oxygen fugacity [22].

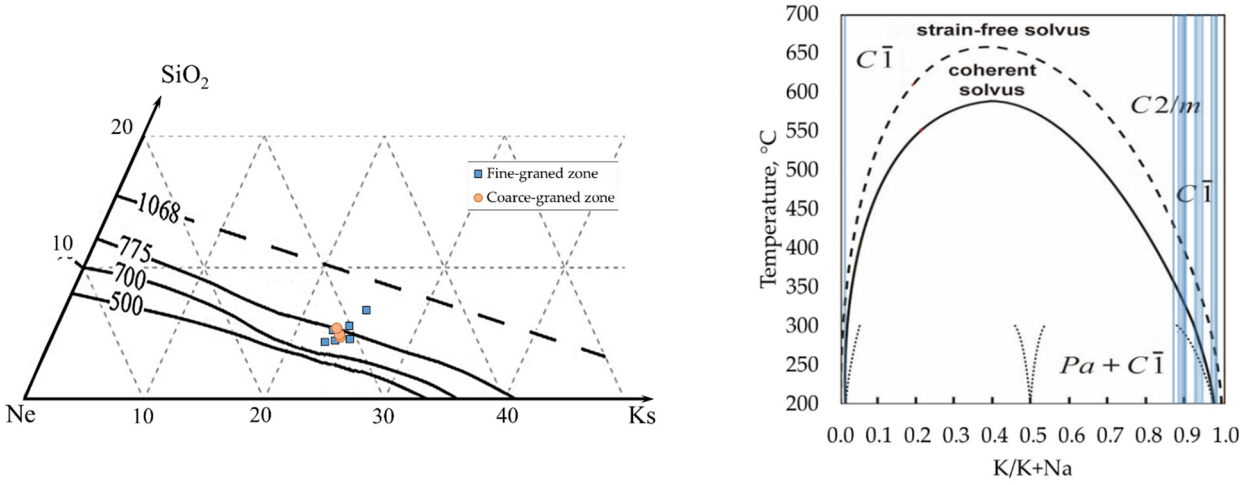

(**a**) (**b**)

Figure 9. Nepheline and feldspar geothermometer for the peralkaline pegmatite of Odikhincha (**a**). The solvus lines (**b**) Isotherms of the solution were taken from Refs [41–43].

In the Ilimaussak massif, taseqite is associated with albite, aegirine, analcime, ancylite-, calcite, dolomite, catapleite, fluorapatite and pectolite, in a late hydrothermal cavity of the albite vein [37]. In the Pilansberg Massif, minerals of the lamprophyllite group transitional to taseqite are found together with barytolamprophyllite [36]. "Taseqite" in the Khibiny massif is considered to be the result of low-temperature replacement of eudialyte and is associated with lovozerite-like mineral, titanite, Sr-rich lamprophyllite (formed after Sr-Ba lamprophyllite), Sr-apatite, pectolite, fersmanite, calcium pyrochlore and loparite [35].

The spatial association of pegmatite with carbonatite requires a comparison with the "agpaitic crossed pegmatites" of the Kovdor massif. However, in the "crossing pegmatites"of the Kovdorsky massif (as well as the Inagli agpaitic pegmatites, less studied but similar to the Kovdorsky ones) the influence of the carbonate environment is expressed in the presence of high-calcium representatives of the eudialyte group, including those containing CO_3^{2-} groups: feklichevite $Na_{11}Ca_9Fe_2Zr_3NbSi_{25}O_{73}(OH,H_2O,Cl,O)_5$, golyshevite $Na_{10}Ca_9Fe_2Zr_3NbSi_{25}O_{73}(OH)_3[CO_3]\,H_2O$ and mogovidite $Na_9(Ca,Na)_6Ca_6(Fe^{3+},Fe^{2+})_2Zr_3Si_{25}O_{72}(CO_3)(OH,H_2O)_4$ [12,44]. In the contrast, the Odikhincha pegmatite contains a high-strontium rare-metal mineralization, including taseqite-like mineral of the eudialyte group, as well as rinkite, mosandrite, lamprophyllite and Sr-rich apatite mineral.

In the Illimaussak, Pilansberg and Khibiny massifs, taseqite and taseqite-like eudialyte is formed during the hydrothermal stage [35–37] and is accompanied by a mineral association largely similar to the mineral association of the studied pegmatite. Thus, despite being in the complex of alkaline-ultrabasic rocks, the pegmatite of the Odikhincha massif is mineralogically similar to the pegmatites of the agpaite-syenite alkaline massifs [12].

The strontium specificity of pegmatite is apparently evidence of the formation of pegmatite because of the interaction of alkaline-ultrabasic rocks of the massif and concentrated salt fluid rich in strontium, whose existence in alkaline complexes was assumed by B.G. Pokrovsky [18]. The sequence in which the activity of various alkaline earth elements manifests itself at the late stages of the evolution of alkaline-ultrabasic complexes was studied by us using the example of alkaline pegmatites and hydrothermalites of the Kovdor massif [44]. An analysis of the evolutionary series of minerals in these objects shows that the activity of magnesium continuously decreases, the activity of calcium continuously

increases, and the activity of strontium and barium passes through a maximum [45]. A similar behavior of barium was observed by us in late differentiates of alkaline rocks of the Khibiny massif. In the crystals of minerals of the thomsonite-Ca–thomsonite-Sr series from hydrothermalites of the Khibiny massif, zones enriched in Sr are noted, marking the stage of high activity of this element [46]. It can be assumed that the crystallization of taseqite and odikhinchaite in pegmatites of the Odikhincha massif also belongs to this stage.

6. Conclusions

We studied the EGMs from the peralkaline pegmatite, located in the melteigites of a typical alkaline-ultrabasic Odikhincha massif (Polar Siberia). The average composition of EGMs crystals corresponds to the IMMA-approved formula of taseqite. The composition and structure features of the studied EGMs are close to the Sr-Nb EGMs found in nepheline-syenite massifs (Khibiny, Lovozero and Pilansberg).

At the same time, taseqite from Ilimaussak (holotype sample) contains higher contents of niobium, chlorine and strontium than the theoretical taseqite. This difference raises the question of actuality to refine the taseqite formula according to the composition of the holotype specimen.

The intracrystalline composition variations are such that in one crystal, there are are-as that formally correspond to at least three mineral species: taseqite, ferrokentbruksite and eudialyte-sensu stricto or some other Nb-poor mineral. Probably, even those different areas of one crystal belong to different subgroups of the eudialyte group.

The presence of three mineral species, each of which requires both chemical and structural data in a single crystal for its accurate diagnosis, illustrates the inconvenience of the conventional principles of mineralogical nomenclature for eudialytes.

There are 10 cationic positions in the structure of the eudialyte, which allow isomorphism, which leads to the possibility of the existence of at least 1024 mineral species. Today, 30 approved minerals of the eudialyte group are known; the majority of them are described in only one place. In addition, there are data on 28 candidates for approval of the mineral species. So, discovering new minerals and ordering them is the way to establish cumbersome and overcomplicated nomenclature, which will not be useful as a guide for the practical purposes of petrology, geochemistry, exploration and technological mineralogy.

At the same time, there are some clearly similar EGMs sampled in different localities, which it would make sense to unite under one name. If they belonged to the same mineral species, then these groups would have the status of a mineral variety, but they do not belong to the same species. Thus, the mineralogical nomenclature needs a «group-variety» taxon that is similar in its laxity to a "variety" but is not subordinate to the mineral species. It might make sense to retain the word "variety" while adding the name of the group or supergroup to it.

It makes sense to enclose the names of such group varieties in quotation marks, so that when reading them, they can easily be distinguished from mineral species, while the names themselves should not coincide in sound and spelling with the existing mineral species.

For example, strontium-niobium EGM from the Odikhincha, Khibiny, Lovozero and Pilansberg massifs constitutes a specific eudialyte variety that can be called "mono-chlore-taseqite" to distinguish it from taseqite sensu stricto, which was found only in the Ilimaussak massif.

Author Contributions: Fieldwork and sampling, V.A.Z.; photo/SEM/EDX analysis, V.A.Z.; petrographic description, V.A.Z.; powder IR spectra obtaining and interpretation, N.V.C.; crysta chemical analysis, S.M.A.; estimation of mineral-forming conditions and geological interpretation, V.A.Z.; writing—original draft preparation, V.A.Z., N.V.C. and S.M.A.; writing—review and editing, V.A.Z. and S.M.A. All authors have read and agreed to the published version of the manuscript.

Funding: The work was supported by the Grant of the Ministry of Science and Higher Education of the Russian Federation (grant No. 13.1902.21.008, agreement 075-15-2020-802) "Fundamental problems of the development of the mineral resource base of high-tech industry and energy in Russia".

Acknowledgments: We are grateful to V.G. Senin for the assistance in microprobe analysis of minerals and A.N. Lapshin for obtaining and transforming the ATR IR spectra. We are also grateful to Vit Robashkevich, who checked and improved the English language of the article.

Conflicts of Interest: The authors declare no conflict of interest.

References

1. Johnsen, O.; Grice, J.D. The Crystal Chemistry of Eudialyte Group. *Can. Mineral.* **1999**, *37*, 865–891.
2. Johnsen, O.; Ferraris, G.; Gault, R.A.; Grice, J.D.; Kampf, A.R.; Pekov, I.V. The Nomenclature of Eudialyte-Group Minerals. *Can. Mineral.* **2003**, *41*, 785–794. [CrossRef]
3. Rastsvetaeva, R.K.; Chukanov, N.V.; Aksenov, S.M. *Minerals of Eudialyte Group: Crystal Chemistry, Properties, Genesis*; University of Nizhni Novgorod: Nizhniy Novgorod, Russia, 2012; ISBN 978-5-91326-207-3.
4. Aksenov, S.M.; Kabanova, N.A.; Chukanov, N.V.; Panikorovskii, T.L.; Blatov, V.A.; Krivovichev, S.V. The role of local heteropolyhedral substitutions in the stoichiometry, topological characteristics and ion-migration paths in the eudialyte-related structures: A quantitative analysis. *Acta Crystallogr. Sect. B Struct. Sci. Cryst. Eng. Mater.* **2022**, *78*, 80–90. [CrossRef] [PubMed]
5. Rastsvetaeva, R.K.; Chukanov, N.V. Classification of Eudialyte-Group Minerals. *Geol. Ore Depos.* **2012**, *54*, 487–497. [CrossRef]
6. Eggenkamp, H.G.M.; Marks, M.A.W.; Atanasova, P.; Wenzel, T.; Markl, G. Changes in Halogen (F, Cl, Br, and I) and S Ratios in Rock-Forming Minerals as Monitors for Magmatic Differentiation, Volatile-Loss, and Hydrothermal Overprint: The Case for Peralkaline Systems. *Minerals* **2020**, *10*, 995. [CrossRef]
7. Schilling, J.; Wu, F.-Y.; McCammon, C.; Wenzel, T.; Marks, M.A.W.; Pfaff, K.; Jacob, D.E.; Markl, G. The Compositional Variability of Eudialyte-Group Minerals. *Mineral. Mag.* **2011**, *75*, 87–115. [CrossRef]
8. Estrade, G.; Salvi, S.; Béziat, D. Crystallization and Destabilization of Eudialyte-Group Minerals in Peralkaline Granite and Pegmatite: A Case Study from the Ambohimirahavavy Complex, Madagascar. *Mineral. Mag.* **2018**, *82*, 375–399. [CrossRef]
9. Sørensen, H. *The Ilímaussaq Alkaline Complex, South Greenland an Overview of 200 Years of Research and an Outlook*; Meddelelser om Grønland. Geoscience; Museum Tusculanum Press: Copenhagen, Danmark, 2006; ISBN 9788763512718.
10. Osipov, A.S.; Antonov, A.A.; Panikorovskii, T.L.; Zolotarev, A.A. Hydrated CO3-Bearing Analog of Manganoeudialyte from Alkali Pegmatites of the Konder Pluton, Khabarovsk Krai. *Geol. Ore Depos.* **2018**, *60*, 726–735. [CrossRef]
11. Khomyakov, A.P.; Nechelyustov, G.N.; Rastsvetaeva, R.K. Aqualite, a New Mineral Species of the Eudialyte Group from the Inagli Alkaline Pluton, Sakha-Yakutia, Russia, and the Problem of Oxonium in Hydrated Eudialytes. *Geol. Ore Depos.* **2007**, *49*, 739–751. [CrossRef]
12. Chukanov, N.V.; Moiseev, M.M.; Rastsvetaeva, R.K.; Rozenberg, K.A.; Zadov, A.E.; Pekov, I.V.; Golyshevite, K.V.V. $(Na,Ca)_{10}Ca_9Fe_2Zr_3NbSi_{25}O_{72}(CO_3)(OH)_3$ H_2O, and Mogovidite, $Na_9(Ca,Na)_6Ca_6Fe_2Zr_3\square Si_{25}O_{72}(CO_3)(OH,H_2O)_4$—New Minerals of the Eudialyte Group from Agpaitic Pegmatites of Kovdor Massif, Kola Peninsula. *Zap. VMO* **2005**, *134*, 36–47.
13. Verwoerd, W.J.; Viljoen, E.A.; Chevallier, L. Rare Metal Mineralization at the Salpeterkop Carbonatite Complex, Western Cape Province, South Africa. *J. Afr. Earth Sci.* **1995**, *21*, 171–186. [CrossRef]
14. Egorov, L.S. *Ijolite Carbonatite Plutonism (Case History of the Maimecha-Kotui Complexes Northern Siberia)*; Nedra: Saint Petersburg, Russia, 1991.
15. Lipenkov, G.V.; Mashak, M.S.; Kirichenko, V.T.; Larichev, A.I.; Nazarov, D.V.; Bigun, I.V.; Kondakova, E.A.; Khabarov, A.N.; Gerasicheva, A.V.; Zavarzin, I.V. State Geological Map of the Russian Federation. Scale 1: 1,000,000 (Third Generation). Anabar-Vilyui Series. *Sheet R-48—Khatanga Explan. Lett.* **2015**, 398.
16. Arzamastsev, A.A.; Glaznev, V.N.; Arzamastseva, L.V.; Bea, F.; Montero, P. Kola Alkaline Province in the Paleozoic: Evaluation of Primary Mantle Magma Composition and Magma Generation Conditions. *Russ. J. Earth Sci.* **2001**, *3*, 1–32. [CrossRef]
17. Salnikova, E.B.; Chakhmouradian, A.R.; Stifeeva, M.V.; Reguir, E.P.; Kotov, A.B.; Gritsenko, Y.D.; Nikiforov, A.V. Calcic Garnets as a Geochronological and Petrogenetic Tool Applicable to a Wide Variety of Rocks. *Lithos* **2019**, *338–339*, 141–154. [CrossRef]
18. Pokrovsky, B.G. *Crustal Contamination of Mantle Magmas on Evidence of Isotope Geochemistry*; Transaction of GIN RAS; Nauka: Moscow, Russia, 2000; Volume 535, 228p.
19. Bagdasaryan, T.E.; Thomson, S.N.; Latyshev, A.V.; Veselovskiy, R.V.; Zaitsev, V.A.; Marfin, A.E.; Zakharov, V.S.; Yudin, D.S. Thermal History of the Siberian Traps Large Igneous Province Revealed by New Thermochronology Data from Intrusions. *Tectonophysics* **2022**, *836*, 229385. [CrossRef]
20. Gritsenko, Y.D.; Chukanov, N.V.; Aksenov, S.M.; Pekov, I.V.; Varlamov, D.A.; Pautov, L.A.; Vozchikova, S.A.; Ksenofontov, D.A.; Britvin, S.N. Odikhinchaite, $Na_9Sr_3[(H_2O)_2Na]Ca_6Mn_3Zr_3NbSi(Si_{24}O_{72})O(OH)_3(CO_3)\cdot H_2O$, a New Eudialyte-Group Mineral from the Odikhincha Intrusion, Taimyr Peninsula, Russia. *Minerals* **2020**, *10*, 1062. [CrossRef]
21. Rastsvetaeva, R.K.; Chukanov, N.V.; Zaitsev, V.A.; Aksenov, S.M.; Viktorova, K.A. Crystal Structure of Cl-Deficient Analogue of Taseqite from Odikhincha Massif. *Crystallogr. Rep.* **2018**, *63*, 349–357. [CrossRef]
22. Nielsen, T.F.D. The Occurrence and Formation of Ti-Aegirines in Peralkaline Syenites. *Contrib. Mineral. Petrol.* **1979**, *69*, 235–244. [CrossRef]
23. Rass, I.T. Trace Element Fractionation in Coexisting High- and Low-Ca Alkali Ultramafic Series of the Odikhincha Massif (Polar Siberia). *Geochem. Int.* **2004**, *42*, 744–754.

24. Mann, U.; Marks, M.; Markl, G. Influence of Oxygen Fugacity on Mineral Compositions in Peralkaline Melts: The Katzenbuckel Volcano, Southwest Germany. *Lithos* **2006**, *91*, 262–285. [CrossRef]
25. Shubin, I.I.; Filina, M.I.; Kogarko, L.N. Evolution of Pyroxenes of the Lovozero Rare Metal Deposit (Lower Zone). *Geochem. Int.* **2021**, *59*, 92–98. [CrossRef]
26. Andersen, T.; Elburg, M.; Erambert, M. Contrasting Trends of Agpaitic Crystallization in Nepheline Syenite in the Pilanesberg Alkaline Complex, South Africa. *Lithos* **2018**, *312–313*, 375–388. [CrossRef]
27. Schonenberger, J.; Markl, G. The Magmatic and Fluid Evolution of the Motzfeldt Intrusion in South Greenland: Insights into the Formation of Agpaitic and Miaskitic Rocks. *J. Petrol.* **2008**, *49*, 1549–1577. [CrossRef]
28. Marks, M.A.W.; Markl, G. The Ilímaussaq Alkaline Complex, South Greenland. In *Layered Intrusions (Springer Geology)*; Charlier, B., Namur, O., Latypov, R., Tegner, C., Eds.; Springer: Dordrecht, The Netherlands, 2015; pp. 649–691. [CrossRef]
29. Zaitsev, V.A.; Kogarko, L.N. Compositions of Minerals of the Lamprophyllite Group from Alkaline Massifs Worldwide. *Geochem. Int.* **2002**, *40*, 313–322.
30. Borst, A.M.; Finch, A.A.; Friis, H.; Horsburgh, N.J.; Gamaletsos, P.N.; Goettlicher, J.; Steininger, R.; Geraki, K. Structural State of Rare Earth Elements in Eudialyte-Group Minerals. *Mineral. Mag.* **2020**, *84*, 19–34. [CrossRef]
31. Mikhailova, J.A.; Stepenshchikov, D.G.; Kalashnikov, A.O.; Aksenov, S.M. Who Is Who in the Eudialyte Group: A New Algorithm for the Express Allocation of a Mineral Name Based on the Chemical Composition. *Minerals* **2022**, *12*, 224. [CrossRef]
32. Chukanov, N.V. *Infrared Spectra of Mineral Species*; Springer: Dordrecht, The Netherlands, 2014; ISBN 978-94-007-7127-7.
33. Rastsvetaeva, R.K.; Chukanov, N.V.; Lisitsin, D.V.; Voronin, M.V.; Varlamov, D.A. Crystal Structure and Indicatopy Significance of Odikhinchaite from the Khibiny Alkaline Complex. *Vestn. Geosci.* **2021**, *4*, 3–9. [CrossRef]
34. Ekimenkova, I.A.; Rastsvetaeva, R.; Khomyakov, A.P. Refinement of the Crystal Structure of a Fe, Sr-Analogue of Kentbrooksite. *Crystallogr. Rep.* **2000**, *45*, 1010–1013. [CrossRef]
35. Azarova, Y.V. Minerals of the Eudialyte Group and Their Alteration Products as a Geochemical Indicator of Postmagmatic Processes during the Formation of the Lujavrite-Malignite Complex in the Khibiny Massif. *Geochem. Int.* **2005**, *43*, 715–720.
36. Mitchell, R.H.; Liferovich, R.P. Subsolidus Deuteric/Hydrothermal Alteration of Eudialyte in Lujavrite from the Pilansberg Alkaline Complex, South Africa. *Lithos* **2006**, *91*, 352–372. [CrossRef]
37. Petersen, O.V.; Johnsen, O.; Gault, R.A.; Niedermayr, G.; Grice, J.D. Taseqite, a New Member of the Eudialyte Group from the Ilímaussaq Alkaline Complex, South Greenland. *Neues Jahrb. Mineral. Mon.* **2004**, *2004*, 83–96. [CrossRef]
38. Yagi, K.; Kikuchi, T.; Kakuta, H. Thermal Decomposition of Pectolite and Its Hydrothermal Synthesis. *J. Fac. Sci. Hokkaido Univ. Ser. 4 Geol. Mineral.* **1968**, *14*, 123–134.
39. Edgar, A.D. Studies on Cancrinites; Part 2, Stability Fields and Cell Dimensions of Calcium and Potassium-Rich Cancrinites. *Can. Mineral.* **1964**, *8*, 53–67.
40. Sirbescu, M.; Jenkins, D.M. Experiments on the Stability of Cancrinite in the System Na_2O–CaO–Al_2O_3–SiO_2–CO_2–H2O. *Am. Mineral.* **1999**, *84*, 1850–1860. [CrossRef]
41. Hamilton, D.L. Nephelines as Crystallization Temperature Indicators. *J. Geol.* **1961**, *69*, 321–329. [CrossRef]
42. Hamilton, D.L.; McKenzie, W.S. Nepheline Solid Solution in the System $NaAlSiO_4$-$KAlSiO_4$-SiO_2. *J. Petrol.* **1960**, *1*, 56–72. [CrossRef]
43. Xu, H.; Jin, S.; Lee, S.; Hobbs, F. Nano-Phase $KNa(Si_6Al_2)O_{16}$ in Adularia: A New Member in the Alkali Feldspar Series with Ordered K–Na Distribution. *Minerals* **2019**, *9*, 649. [CrossRef]
44. Moiseev, M.M.; Chukanov, N.V. Mineralogy of Alkaline Pegmatites and Hydro-Thermalites of the Kovdor Massif. *New Data Miner.* **2006**, *41*, 56–70.
45. Pekov, I.V.; Chukanov, N.V.; Turchkova, A.G. On the Mineralogy and Behavior of Barium in Differentiates of Alkaline Rocks of the Khibiny Massif, Kola Peninsula. In Proceedings of the XIX Russian Meeting "Geochemistry of Igneous Rocks", Moscow, Russia, 6–7 April 2000; pp. 111–112. Available online: https://drive.google.com/file/d/101DuzSzT-SBzxOWC4g-fjNhsjxPSEhdv/view?usp=sharing (accessed on 13 May 2022).
46. Pekov, I.V.; Lovskaya, E.V.; Turchkova, A.G.; Chukanov, N.V.; Zadov, A.E.; Rastsvetaevs, R.K.; Kononkova, N.N. Thomsonite-Sr, $(Sr,Ca)_2Na[Al_5Si_5O_{20}]\cdot 6\text{-}7H_2O$, a New Zeolite from the Khibiny Massif, Kola Peninsula and the Thomsonite-Ca—Thomsonite-Sr Isomorphous Series. *Zap. Ross. Mineral. Obs.* **2001**, *130*, 46–55.